Northumbria
University
NEWCASTLE

Electrically Tuning Characteristics of LC Selectively Infiltrated PCF Sagnac Interferometer

Pingsheng Xue, Qiang Liu, Zhaoxia Wu, Qiang Wu, Chenyu Zhao, Wai Pang Ng, Senior Member, IEEE, Richard Fu, and Richard Binns

***Abstract*—A photonic crystal fiber was selectively infiltrated only two of the air holes near the core with liquid crystal. The selective infiltration caused geometric asymmetry and created high birefringence. Because of the geometric asymmetry, the response to varying electric field is concerned with electric field direction. A Sagnac interferometer was set to investigate the electric tuning characteristics of the selectively infiltrated photonic crystal fiber. The effective refractive-indices of the fiber varies with electric field due to reorientation of liquid crystal molecules. The highest sensitivity was 1.12 nm/V (504 nm/kV/mm) with tuning range of 7 nm when electric field direction was parallel to the connecting line of infiltrated holes. The response time of the selectively infiltrated photonic crystal fiber was studied. The device can be utilized as voltage sensors, electro-optical modulators and filters.**

***Index Terms*—Liquid crystal, Photonic crystal fiber, Sagnac interferometer, Electric field sensing, Modulators.**

I. Introduction

WITH numbers of holes going through it, photonic crystal fiber (PCF) [1] can be infiltrated with various materials. The guiding mechanism can be modulated by infiltrated materials. Photonic crystal fiber based devices such as sensors [2-4], optical filters [5] and polarization switch [6] are realized. Fiber devices are novel, compact, sensitive and quick in response, the researches on fiber devices are popular and numbers of studies on PCF infiltrated with functional materials have been explored in last decade [7]. Nematic liquid crystal (LC) [8] is sensitive to electric field, and it has the fluidity of liquid, which means it can be infiltrated into the air holes of PCF. Once an electric field high enough is applied to the LC infiltrated fiber, the liquid crystal molecules in the air holes will reorient [9,10] which will cause effective refractive indices vary with the electric field. Du et al. displayed an electrically tunable Sagnac filter based on a photonic bandgap fiber with LC infused, with the sensitivity of 0.53 nm/V [11]. Mathews et al. exhibited LC infiltrated PCF for electric field intensity measurements in [12], which has sensitivity of 10.1 dB per kV_{rms}/mm. Yang et al. realized an electrically tunable micro resonator based on LC-infiltrated PCF with the sensitivity of 0.01 nm/V [13]. Above research are based on entirely infiltrated PCFs, which are easy to realize. The guiding mechanisms usually change from total internal reflection (TIR) to photonic bandgap (PBG) effect if all air holes are infiltrated with materials whose refractive indices are higher than background. However, if only a few specific holes are infiltrated with higher index materials, the guiding mechanism does not change to PBG directly but brings diverse properties [14-20], such as multiwaveguide coupling [14] or high birefringence induced by asymmetry infiltration [15]. Selectively infiltrated PCFs confining light by both index-guiding and bandgap-guiding was introduced in [16]. LC selectively infiltrated polarization maintaining PCF for electric field sensing with the sensitivity of 2 dB per kV_{rms}/mm was studied in [18]. Huang et al. realized a high-sensitivity voltage sensor based on PCF with one hole infiltrated with LC and the sensitivity was up to 5.594 nm/V [14]. Selective infiltration provides various ways to improve sensing characteristics.

In this paper, a Sagnac interferometer based on PCF with LC selectively infiltrated into two opposite holes adjacent to the core is carried out. Compared with previous works, with the advantage of asymmetry, not only electric field intensity but also the direction were considered. The dips red shift with increasing voltage from 160 to 190 V and the sensitivity reaches highest of 1.12 nm/V (504 nm/kV/mm) from 182 to 186 V when the connecting line of infiltrated holes is parallel to the electric field direction. While the dips slightly blue shift when it is perpendicular to the electric field. The device shows electric field direction tunable characteristics, dynamic range and sensitivity can be adjusted. In addition to measuring electric field intensity, it is possible to detect the direction of the field in practice.

II. Principle and Experiment Setup

The PCF used in our experiment was SM-10 (Fig. 1). The air hole diameter is 4 μm, core diameter is 10 μm and lattice size is 6 μm. The background material is silica glass. Only two opposite air holes adjacent to the core were infiltrated with nematic LC. The method to realize selective infiltration was blocking irrelevant air holes with UV curing

Manuscript received ××, 2021; revised ××, 2021; accepted ××, 2021. This work was supported in part by the National Natural Science Foundation of China under Grant 51907017, in part by the Key Science and Technology Research Projects of Higher Education Institutions in Hebei Province of China under Grant ZD2019304, in part by the Fundamental Research Funds for the Central Universities of China under Grant N182304011, and in part by the China National Fund for Studying Abroad. *(Corresponding author: liuqiang@neuq.edu.cn)*

Pingsheng Xue, Qiang Liu, Zhaoxia Wu, and Chenyu Zhao are with the State Key Laboratory of Synthetical Automation for Process Industries, School of Control Engineering, Northeastern University at Qinhuangdao, Qinhuangdao 066004, China (e-mail: 1901906@stu.neu.edu.cn; liuqiang@neuq.edu.cn; ysuwzx@126.com; 1871708@stu.neu.edu.cn).

Qiang Wu, Wai Pang Ng, Richard Fu, and Richard Binns are with the Faculty of Engineering and Environment, Northumbria University, Newcastle upon Tyne NE1 8ST, U.K. (e-mail: qiang.wu@northumbria.ac.uk; wai-pang.ng@northumbria.ac.uk; richard.fu@northumbria.ac.uk; richard.binns@northumbria.ac.uk).

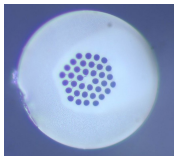

Fig. 1. Cross section of the PCF, 3 layers, the core diameter is 10 μm , air hole diameter is 4 μm, lattice size is 6 μm.

adhesive [17]. The length of the PCF was ∼4 cm, about 8 mm of the PCF was filled with LC, overlong LC would cause more transmission loss. LC does not flow in capillary so the empty section have no influence on experiment. LC is a kind of anisotropic material; the ordinary and extraordinary refractive index can be represented as n_o and n_e. The nematic LC used in our experiment was E7 liquid crystal, indices are $n_e = 1.6693 + (0.0085/\lambda^2) + (0.0027/\lambda^4)$, $n_o = 1.4998 + (0.0067/\lambda^2) + (0.0004/\lambda^4)$ [19].

The unfilled hexagonal symmetric PCF has extremely low birefringence, however, if some of the air holes are filled with materials, the structure is not symmetric anymore, high birefringence is induced. In this experiment, since only two opposite air holes adjacent to the core are infiltrated with LC whose refractive index is higher than background, the index of x-polarization in Fig. 2(a) will be higher than that in y-polarization. Mode effective indices after infiltration were calculated by finite element method to have an estimate, modes guided in core are plotted in Fig. 2(b), birefringence is induced and x- have higher indices than y-polarization. The nematic LC molecules in capillary will align with its long axis parallel to the fiber axis when electric field is below a threshold intensity.

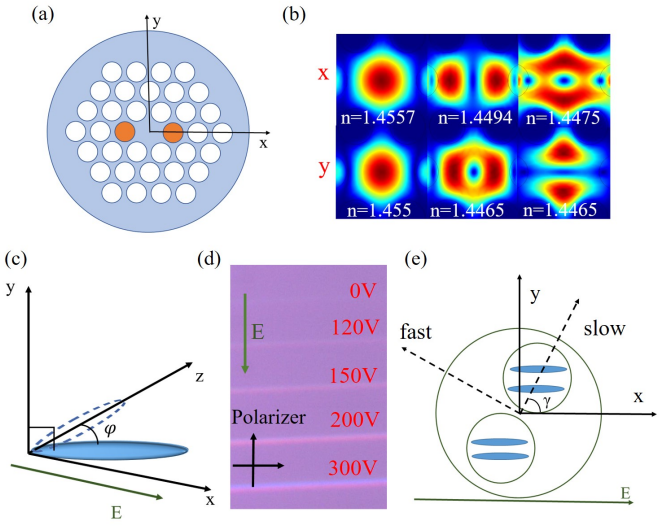

Fig. 2. (a) Two opposite air holes adjacent to the core are infiltrated with LC, the connecting line of the two hole centers is named as slow axis. (b) Distribution and calculated effective indices of modes guided in core at 1630 nm after infiltration. (c) LC molecules tilt to electric field direction. (d) Observed by polarization microscope, LC molecules tilt in electric field and have angles between two orthogonal polarizers, it becomes brighter when voltage increases. (e) LC molecular alignment on applying of electric field with angle to the connecting line of the centers of the infiltrated holes (slow axis).

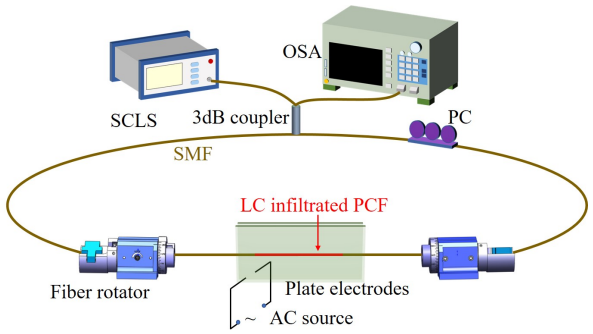

Fig. 3. Schematic of the Sagnac interferometer based on LC selectively infiltrated PCF.

Once electric field above the threshold is applied, the LC molecules will tilt an angle in the electric field direction and the angle will increase with the electric field intensity (Fig. 2(c)), which will cause changes in mode effective indices of the PCF. Fig. 2(d) shows LC tilt in a capillary with increasing electric field. It becomes brighter observed by polarization microscope when LC molecules tilt to electric field direction and have an angle between the polarizers. If electric field is in x-direction in Fig. 2(c), the relation of tilt angle φ and permittivity of diagonal tensor $\varepsilon = [\varepsilon_{xx}, \varepsilon_{yy}, \varepsilon_{zz}]$ is expressed as $\varepsilon_{xx} = \varepsilon_e \sin^2\varphi + \varepsilon_o \cos^2\varphi, \varepsilon_{yy} = \varepsilon_o, \varepsilon_{zz} = \varepsilon_o \sin^2\varphi + \varepsilon_e \cos^2\varphi$; The index of x increases with electric field intensity while the index is almost constant in y. The connecting line of the centers of infiltrated holes was named as slow-axis and the orthogonal direction fast-axis in this paper. In Fig. 2(e), if electric field is applied with an angle γ to the slow axis, the LC index components in slow and fast axes can be calculated by $n^2_{\mathrm{LCs}} = \mathrm{n}^2_{\mathrm{x}} \cos^2\varphi + \mathrm{n}^2_{\mathrm{y}} \sin^2\varphi$, $n^2_{\mathrm{LCf}} = \mathrm{n}^2_{\mathrm{y}} \cos^2\varphi + \mathrm{n}_{\mathrm{x}} \sin^2\varphi$. When the electric field intensity is constant, the LC index component in slow axis decrease while fast axis component increases as γ changes from 0 to 90°. As a result, the mode effective refractive indices of the LC infiltrated PCF will vary with the angle γ. Fig. 3 shows the schematic of Sagnac interferometer experiment setup. Light from supercontinuous light source (SCLS) is split equally into two beams by a 3 dB coupler and propagate clockwise and counterclockwise in the loop. Due to the birefringence of the LC infiltrated PCF, phase difference occurred and caused interference when they transmit back to the coupler. Polarization controller (PC) can rotate the polarization direction to optimize interference spectrum displayed on the optical spectrum analyzer (OSA). The birefringence of the LC infiltrated PCF can be modulated by electric field intensity and direction, and that will cause interference dip shifting. The transmittance of Sagnac interferometer can be described as [4,11,20]:

$$T = \frac{1 - cos(2\pi BL/\lambda)}{2} \quad (1)$$

L represents the length of LC section, $B = |n_{\mathrm{fast}} - n_{\mathrm{slow}}|$ is the birefringence. The interference dips will appear when $2\pi BL/\lambda = 2m\pi$, m is an integer. The distance between two electrodes was 450 μm in order to make sure the fiber could rotate without grazing the electrodes. The experiment was carried out at room temperature of 20°C.

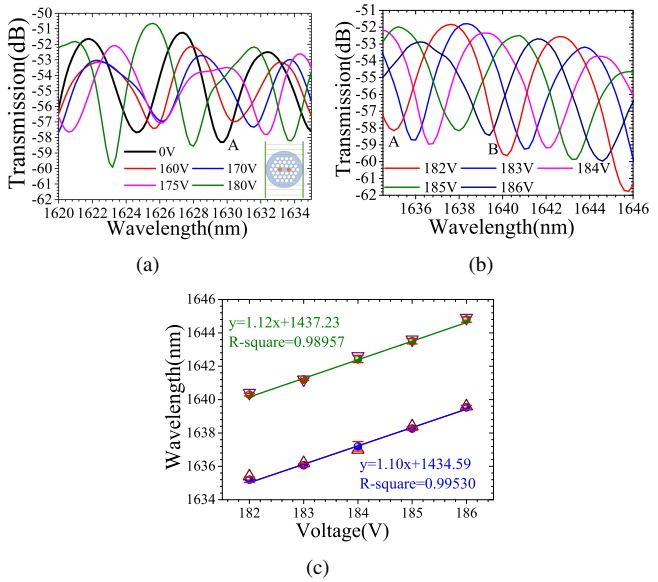

Fig. 4. Spectrum of 0 V and dips red shift as voltage increased (a) from 160 to 180 V and (b) from 182 to 186 V when $\gamma = 0°$. (c) Linear fitting results of the relations between voltages and dip wavelengths, error bars are calculated from 4 times repeated tests, the hollow triangle dots are reverse tests, can be considered no hysteresis.

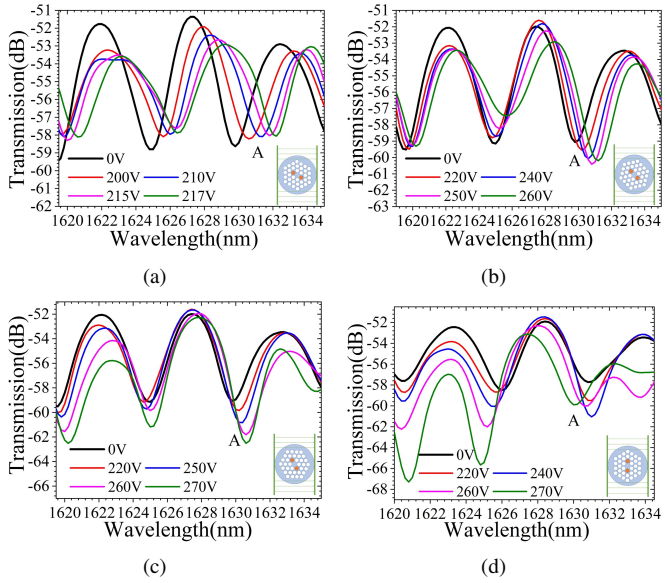

Fig. 5. Dips red shift as voltage increased when (a) $\gamma = 30°$ (b) $\gamma = 45°$ (c) $\gamma = 60°$. As γ increased, the sensitivity decreased, while (d) $\gamma = 90°$, the dips bule shift with increasing voltage.

TABLE I
COMPARISON BETWEEN OURS AND PREVIOUS WORKS

Ref.	LC	Distance	Fiber	Sensitivity
[11]	MDA	125μm	– –	0.53nm/V
[13]	BHR	130μm	MOF	0.01nm/V
[14]	E7	130μm	ESM-12	5.594 nm/V
[18]	MLC	150μm	PM-1550	20dB/kV/mm
[21]	MLC	125μm	LMA-10	1.6nm/V
[22]	E7	– –	LMA-8	1.8nm/V
Ours	E7	450μm	SM-10	1.12nm/V

III. Results and Discussion

Interference dips can be seen from 1620 to 1660 nm. At first, the slow axis was parallel to the electric field, the angle $\gamma = 0°$ (Fig. 4(a) inset). We increased the voltage gradually, the spectrum had no obvious change until the voltage reached 150 V. As the voltage was further increased from 160 to 180 V, the dip started to shift to right. Fig. 4(b) shows as the voltage increased from 182 to 186 V, dip A and B red shifted by 6.3 and 7 nm. And linear fitting of the relations between dip wavelengths and voltages are shown in Fig. 4(c), the slopes indicate the sensitivities of the two dips reached 1.10 nm/V and 1.12 nm/V, linearities are 0.99530 for dip A and 0.98957 for B. The repeatability and reversibility are satisfactory. We continued increasing voltage, the interference can not be observed over 190 V, so the voltage upper limit for $\gamma = 0°$ was 190 V. Performance of relevant studies are listed in Table I, our sensitivities are competitive among them.

When the LC infiltrated PCF was rotated 30° and 45°, like Fig. 5(a)(b) inset shows, the shift of the dips was relatively not as obvious as 0°. Fig. 5(a) shows the spectrum when γ was 30° and voltage increased to 217 V. The sensitivity was lower than that of 0°. When it was set in 45°, as Fig. 5(b) shows, for voltage increment of 40 V (from 220 to 260 V), the shift was about only 1 nm. When $\gamma = 60°$, though the voltage increased significantly, the shift of dips was tiny, shifts were inconspicuous even the voltage reached 270 V (Fig. 5(c)). While $\gamma = 90°$, the slow axis was perpendicular to the electric field direction, the LC molecules would tilt parallel to the fast axis direction. The spectrum is shown in Fig. 5(d). It could be found not only the transmission intensity decreased but also the dips blue shifted slightly, which was different with 0°, 30°, 45° and 60°. Fig. 6 reveals dip A shift with increasing voltage at different degrees. When $\gamma = 0°$, red shift was the most obvious, because the LC molecules tilted along slow axis and further increases the effective refractive index of slow axis, birefringence changed greatest compared with other angles at the same voltage. As γ increasing, the LC index increment component in slow axis was decreasing while the component in fast axis was increasing, so the sensitivity was becoming lower because the birefringence increment was less, when $\gamma = 60°$, the dips hardly shift with increasing voltage. While the LC infiltrated PCF rotated 90°, the dips shifted to opposite direction. The reason is that the LC molecules tilt along fast axis, the effective refractive index of fast axis increases most while the slow axis least, which lead to the

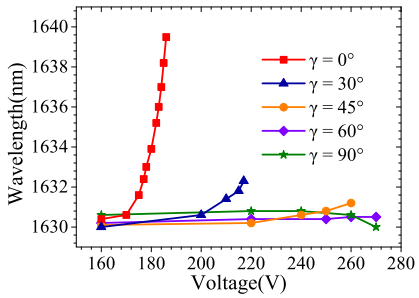

Fig. 6. The dip wavelength shifts with increasing voltage at different angles.

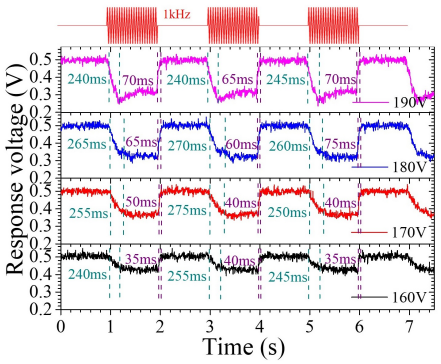

Fig. 7. Response times at different voltages, when $\gamma = 0°$.

reduction of birefringence as voltage becomes higher. The asymmetric infiltration structure showed directional tunable characteristics, which has the potential to detect the field direction in practice. The transmission intensity declined as voltage rose because more light attenuated in LC and caused decrease in the power transmitted in core. When γ was low, polarization in slow axis tend to extinct first as voltage rising because of the increasing LC indices along slow axis, for this reason the dynamic range was restricted. As γ increased, the voltage upper limit extended. The sensitivity was not linear in wide range, it is more sensitive at higher voltage. That was because the molecules began to overcome the effect of thermal motion and anchoring energy and rotate more easily. Temperature influence the indices of LC significantly [19] so the device needs recalibration when temperature changes.

Response times of the LC infiltrated PCF were investigated with a photodetector and an oscilloscope. 1 kHz sinusoidal signal with switching period of 1 second was applied to the LC infiltrated PCF, γ was 0°. The responses at different voltage are shown in Fig. 7. The lower response voltages at higher applied voltages indicated the loss increased with applied voltage. The average response times are about 250 ms. Recover times are about 35∼40 ms at 160 V and 65∼70 ms at 190 V. The device can be used as a sensor as well as an optical switch.

IV. Conclusion

Electric field intensity and direction tuning characteristics of the Sagnac interferometer based on PCF with LC infiltrated into two opposite air holes adjacent to the core were investigated. When the two-hole centers connecting line is parallel with the electric field direction ($\gamma = 0°$), the interference dips red shift with increasing voltage and it has the highest sensitivity from 182 to 186 V in our experiment, which is 1.12 nm/V (504 nm/kV/mm). As the angle increases, the sensitivity declines and when it is perpendicular to electric field direction ($\gamma = 90°$), the dips blue shift with increasing voltage. The sensing characteristics of selective asymmetric infiltration shows the ability to be tuned by electric field direction. Response time of the fiber was measured. The device has the possibility to be used as an electric field or voltage sensor, electro-optical modulator, filter, or optical switch.

References

[1] P. S. J. Russell, "Photonic crystal fibers," Science, vol. 299, no. 5605, pp. 358-362, Jan. 2003.
[2] Q. Liu, P. Xue, and Z. Liu, "Voltage sensor based on liquid-crystal-infiltrated photonic crystal fiber with high index," Appl. Phys. Express, vol. 13, no. 3, p. 032005, Feb. 2020.
[3] Q. Liu, L. Xin, and Z. Wu, "Refractive index sensor of a photonic crystal fiber Sagnac interferometer based on variable polarization states," Appl. Phys. Express, vol. 12, no. 6, p. 062009, May 2019.
[4] Q. Liu, L. Xing, S. Yan, L. Lv, and Z. Liu, "Sensing characteristics of photonic crystal fiber Sagnac interferometer based on novel birefringence and Vernier effect," Metrologia, vol. 57, no. 3, p. 035002, May 2020.
[5] M. Chang, B. Li, N. Chen, X. Lu, X. Zhang, and J. Xu, "A compact and broadband photonic crystal fiber polarization filter based on a plasmonic resonant thin gold film," IEEE Photon. J., vol. 11, no. 2, pp. 1-12, Apr. 2019.
[6] D. Zografopoulos, A. Pitilakis, and E. Kriezis, "Dual-band electro-optic polarization switch based on dual-core liquid-crystal photonic crystal fibers ," Appl. Opt., vol. 52, no. 26, pp. 6439-64440, Sep. 2013.
[7] J. Algorri, D. Zografopoulos, A. Tapetado, D. Poudereux and J.Snchez-Pena. "Infiltrated Photonic Crystal Fibers for Sensing Applications" Sensors-Basel., vol. 19, no. 2, p.4263, Dec. 2018.
[8] C. P. Lapointe, T. G. Mason, and I. I. Smalyukh, "Shape-controlled colloidal interactions in nematic liquid crystals," Science, vol. 326, no. 5956, pp. 1083-1086, Nov. 2009.
[9] L. Scolari, T. Alkeskjold, J. Riishede, A. Bjarklev, D. Sparre Hermann, Anawati, M. Nielsen, and P. Bassi "Continuously tunable devices based on electrical control of dual-frequency liquid crystal filled photonic bandgap fibers," Opt. Express. vol. 13, no. 19, pp.7483-7496, Sep. 2005.
[10] D. Budaszewski, M. Chychlowski, A. Budaszewska, B. Bartosewicz, B. Jankiewicz, and T. R. Wolinski, "Enhanced efficiency of electric field tunability in photonic liquid crystal fibers doped with gold nanoparticles," *Opt. Express*, vol. 27, no. 10, pp. 14260-14269, May 2019.
[11] J. Du, Y. Liu, Z. Wang, B. Zou, B. Liu, and X. Dong, "Electrically tunable Sagnac filter based on a photonic bandgap fiber with liquid crystal infused," Opt. Lett., vol. 33, no. 19, pp. 2215-2217, Sep. 2008.
[12] S. Mathews, G. Farrell, and Y. Semenova, "Liquid crystal infiltrated photonic crystal fibers for electric field intensity measurements," Appl. Opt., vol. 50, no. 17, pp. 2628-2635, Jun. 2011.
[13] C. Yang, H. Zhang, B. Liu, Y. Li, and H. Liu, "Electrically tunable whispering gallery mode microresonator based on a grapefruit microstructured optical fiber infiltrated with nematic liquid crystals," Opt. Lett., vol. 42, no. 15, pp. 2988-2991, Jul. 2017.
[14] Y. Huang, Y. Wang, L. Zhang, Y. Shao, F. Zhang, C. Liao, and Y. Wang, "Tunable electro-optical modulator based on a photonic crystal fiber selectively filled with liquid crystal," J. Lightwave Technol., vol. 37, no. 9, pp. 1903-1908, Jan. 2019.
[15] J. Ma, H. H. Yu, X. Jiang, and D. S. Jiang, "High-performance temperature sensing using a selectively filled solid core photonic crystal fiber with a central air-bore," Opt. Express, vol. 25, no. 8, pp. 9406-9415, Apr. 2017.
[16] L. Xiao, W. Jin, and M. S. Demokan, "Photonic crystal fibers confining light by both indexguiding and bandgap-guiding: hybrid PCFs," Opt. Express, vol.15, no. 24, 15637C15647, Nov 2007.
[17] K. Li, M. Jiang, Z. Zhao, Z. Wang, "Low coherence technique to interrogate optical sensors based on selectively filled double-core photonic crystal fiber for temperature measurement," Opt. Commun, vol. 389, pp. 234-238, Apr. 2017.
[18] S. Mathews, G. Farrell, and Y. Semenova, "All-fiber polarimetric electric field sensing using liquid crystal infiltrated photonic crystal fibers," Sensor. Actuat. A-Phys., vol. 167, no. 1, pp. 54-59, May 2011.
[19] J. Li, S. Wu, S. Brugioni, R. Meucci, and S. Faetti, "Infrared refractive indices of liquid crystals," J. Appl. Phys., vol. 97, no.7, p. 073501, Apr. 2005.
[20] Y. Liu, B. Liu, X. Feng, W. Zhang, G. Zhou, S. Yuan, G. Kai, and X.i Dong, "High-birefringence fiber loop mirrors and their applications as sensors," Opt. Lett., vol. 35, no. 10, pp. 1608-1610, May. 2010.
[21] L. Wei, T. T. Alkeskjold, and A. Bjarklev, "Electrically tunable bandpass filter using solid-core photonic crystal fibers filled with multiple liquid crystals," Appl. Optics., vol. 44, no. 12, pp. 2382-2390, Apr. 2005.
[22] C. H. Lee, C. H. Chen, C. L. Kao, C. P. Yu, S. M. Yeh, W. H. Cheng, and T. H. Lin, "Photo and electrical tunable effects in photonic liquid crystal fiber," *Opt. Express*, vol. 18, no. 3, pp. 2814-2821, Jan. 2010.